DOI: 10.48011/asba.v2i1.1327

Comparative Study of Different Values of Inertia for Islanded Systems ⋆

Fábio A. L. Alves * **Thiago F. S. Costa** **
Bruno M. Laurindo * **João A. V. C. Costa** * **Maurício Aredes** *

* *LEMT, Instituto Alberto Luiz Coimbra de Pós Graduação e Pesquisa de Engenharia, Universidade Federal do Rio de Janeiro, UFRJ, RJ, (e-mail: fabioleitealves@lemt.ufrj.br, brunoml@lemt.ufrj.br, joao@lemt.ufrj.br, aredes@lemt.ufrj.br).*
** *Operador Nacional do Sistema Elétrico - ONS, RJ, (e-mail: tcosta@ons.org.br)*

Abstract: This work presents challenges related to voltage and frequency control for different values of inertia in islanded systems. The mathematical and physical basis of the problem are explained and, after that, a fictional rural network is proposed. The rural network is islanded from the utility grid and then analysed for differents types of generation and inertia values. Frequency and voltage of the network are compared. The results of this work enforce that firm energy generation and the sources inertia are extremally important for the islanded network's stability and safety.

Keywords: Rotating Inertia, Distributed Generation, Microgrids, Photovoltaic Systems, Islanded Systems

1. INTRODUCTION

The necessity to diversify the energy matrix, coupled with the growth of renewable energy sources, promotes changes in the classical power systems topology. Also, financial incentives from regulatory agencies tend to accelerate this growth and penetration of alternative sources. The so-called distributed generation (DG) appears in this context.

In this scenario of DG, the concept of microgrids appear, where the performance of the inverters, an important part of the system, has also been evolving. Voltage source inverters (VSIs) are often used as a power electronic interface; therefore, the control of parallel VSIs that form a microgrid has been investigated in recent years (Vasquez et al., 2010), (Green and Prodanović, 2007), (Pogaku et al., 2007), (Teodorescu et al., 2006), (Delghavi and Yazdani, 2011), (Sao and Lehn, 2008), (Barklund et al., 2008), (Majumder et al., 2009), (Katiraei and Iravani, 2006).

The spread of DGs makes the existence and operation of microgrids possible. If a disturbance or a fault occurs in the utility grid, a part of it can be disconnected and operate autonomously and reconnect after the problem is solved. The economic factor also leads to the emergence of microgrids, where at peak times it can be cheaper to disconnect and use the region's DG.

However, the islanded operation requires caution, because the autonomous region can suffer from frequency and voltage fluctuations caused by faults or load disturbances. The main reason for this behavior are low inertia values of the synchronous generators and the significant presence of renewable sources connected via power electronics converters. These converters lack intrinsic inertial responsiveness, and connected in large quantities can cause the system to become unstable (Dag and Mirafzal, 2016). To protect the islanded system, the connected equipment and ensure power quality supplied to the customers, Brazilian regulatory agency ANEEL (from portuguese, *Agência Nacional de Energia Elétrica*) stipulated the operating limits of operation for voltage and frequency (ANEEL, 2018).

This paper aims to evaluate the influence of different values of rotating inertia on the frequency and voltage profiles of islanded systems. To achieve this objective, a fictitious rural distribution system was simulated, with two DGs connected at the end of their feeders. These DGs were modeled as small hydroelectric plants (SHP) or as photovoltaic systems (PVS). The combination of cases with two SHP and one SHP with one PVS provides different values of equivalent inertia to study the proposed case.

The work is divided as follows: Section II explains the fundamental theory of rotating inertia and its impact on electrical systems; Section III details the rural distribution system, as well as the synchronous generator model, its speed governor, its voltage regulator, and the PVS model; Section IV presents the simulation results, in addition to the discussion about them; and Section V concludes the study.

2. STABILITY IN ISLANDED SYSTEMS

Power systems stability is a classical problem in electrical engineering, being deeply discussed and published

⋆ This study was financed in part by the Coordenação de Aperfeiçoamento de Pessoal de Nível Superior - Brasil (CAPES) - Finance Code 001.

in technical literature. This analysis becomes even more important in the context of islanded systems. Being disconnected from the main system, the microgrid becomes more susceptible to instabilities due to short circuits and large load variations (Tielens and Van Hertem, 2012). Rotating inertia's influence in frequency and voltage stability is mathematically described in the following subsections.

2.1 Frequency Stability

The basic equation that governs angular and frequency stability is exposed in (1). This equation is known as the Swing Equation of the Synchronous Generator, and it relates the system's frequency (ω), mechanical power at generator's shaft (P_m), electrical power (P_e), the machine intrinsic damping (D) and inertia constant (H). The demonstration of this equation is widely known and can be found in (Kundur et al., 1994).

$$\frac{\mathrm{d}\omega}{\mathrm{d}t} = \frac{1}{2H}[P_m - P_e - D\omega] \tag{1}$$

The inertia constant H is defined as:

$$H = \frac{1}{2}\frac{J\omega_m^2}{S_{base}} \tag{2}$$

Where J is the rotor's moment of inertia, ω_m is the mechanical angular speed, and S_{base} is the generator rated apparent power. Equation (2) can be understood as the ratio between the stored rotational kinetic energy by the generator's electrical capacity.

In a few words, (1) relates the load-generation balance with the mechanical speed of the machine, and consequently, the electrical frequency of the system. Considering $D = 0$, a brief analysis can be made: if $P_m > P_e$, the machine will accelerate and may lose the synchronism; the opposite may happen if $P_m < P_e$. If the difference between P_m and P_e is constant, H will determinate the rate of change of shaft's velocity. H is inversely proportional to this rate of change: if the machine has high rotational inertia, the acceleration will be small (Blaabjerg et al., 2006).

2.2 Voltage Stability

Voltage stability is a power system's capability to maintain its buses voltage level within acceptable operating limits, as it can be seen in Kundur et al. (1994). In transmission systems, voltage stability problems can be associated with the lack or excess of reactive power in the grid. Rotor's angle can also generate this type of instability, although this cause is not the most frequent.

In the case of distribution systems, as in the present study, the behavior of voltage levels is different from transmission systems. The main reason for this difference resides in the type of transmission lines and cables used in each case. High voltage transmission systems are mostly inductive, while medium voltage distribution systems and microgrids are either mostly resistive or with the $\frac{X_l}{R}$ ratio close to 1.

For this work's scenario, the classical particular case where variations in active power (P) affect the frequency (f) and variations in reactive power (Q) affect the voltage level (V) is no longer applicable. Equations (3) and (4) exhibit the cross-coupling between system frequency and voltage with the powers and line impedances.

$$f - f_0 = -k_p\frac{X_l}{Z}(P - P_0) + k_q\frac{R}{Z}(Q - Q_0) \tag{3}$$

$$V - V_0 = -k_p\frac{R}{Z}(P - P_0) - k_q\frac{X_l}{Z}(Q - Q_0) \tag{4}$$

Due to the cross-coupling aforementioned equations, variations of P can promote changes on the system voltage levels. Equation (1) shows the direct relationship between H and P. Since in distribution systems P affects the voltage levels, H plays a major role in voltage stability (Zhang et al., 2016).

3. SYSTEM MODELLING

In this work, the mathematical models derived are implemented in Simulight, a simulation software developed by COPPE-UFRJ together with Light Serviços de Eletricidade S.A. It is a software capable of running both power flow studies and power systems dynamics. This work is interested in the dynamic simulations since its objective is to analyze islanded system stability.

The modelled system is a fictional rural distribution system, as can be seen in Figure 1. It has a 69 kV infinite bus that lower its value to 13.8 kV through a substation. Three feeders leaves the substation to supply the consumers. The islanded system will be formed by feeders 1 and 2, and therefore only these will be detailed in this work.

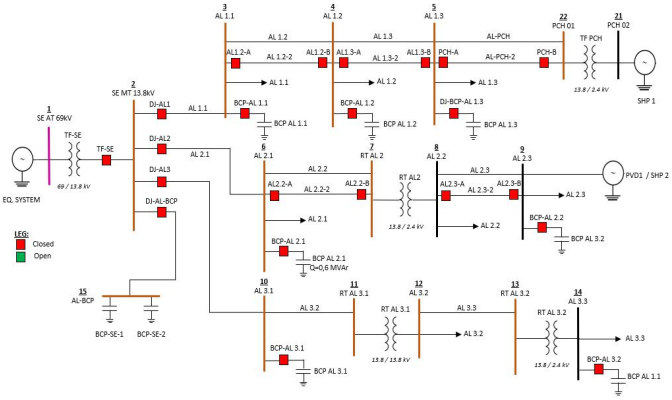

Figure 1. Topology of the rural distribution system.

Feeder 1 has four buses on its extension. The first bus is connected to the next by a single line. The other connections are made using two identical and electrically decoupled lines in parallel. At the end of the feeder, there is an independent producer, connecting a DG by a transformer.

Feeder 2 has a topology similar to Feeder 1, however, it differs from 1 in that it contains a voltage regulator and there are no loads and capacitor banks on the bus of the regulator's high terminal. There is also a DG at the end of this feeder. Tables 1 to 4 exposes all the lines, transformers, loads, and capacitors parameters of both Feeder 1 and Feeder 2.

Table 1. Feeder 1 and 2 Line Parameters.

Line	From Bus	To Bus	V (kV)	R+ (%)	X+ (%)	B+ (%)	R0 (%)	X0 (%)	B0 (%)
Feeder AL 1.1	2	3	13.8	63.45	85.93	0.00	0.00	10.00	0.00
Feeder AL 1.2	3	4	13.8	254.02	182.24	0.00	0.00	20.00	0.00
Feeder AL 1.2-2	3	4	13.8	254.02	182.24	0.00	0.00	20.00	0.00
Feeder AL 1.3	4	5	13.8	254.02	182.24	0.00	0.00	20.00	0.00
Feeder AL 1.3-2	4	5	13.8	254.02	182.24	0.00	0.00	20.00	0.00
AL-PCH	5	22	13.8	0.32	0.42	0.00	0.00	20.00	0.00
AL-PCH-2	5	22	13.8	0.32	0.42	0.00	0.00	20.00	0.00
Feeder AL 2.1	2	6	13.8	79.32	107.41	0.00	0.00	10.00	0.00
Feeder AL 2.2	6	7	13.8	317.53	227.78	0.00	0.00	20.00	0.00
Feeder AL 2.2-2	6	7	13.8	317.53	227.78	0.00	0.00	20.00	0.00
Feeder AL 2.3	8	9	13.8	158.76	113.89	0.00	0.00	10.00	0.00
Feeder AL 2.3-2	8	9	13.8	317.53	227.78	0.00	0.00	20.00	0.00

Table 2. Transformers Parameters.

Transformador	From Bus	To Bus	V (kV)	R (%)	X (%)
TF PCH	22	21	13.8/2.4	15.09	165.98
RT AL2	7	8	13.8/13.8	2.23	28.57

Table 3. Loads from Feeder 1 and 2.

Load	Bus	P (MW)	Q (Mvar)
AL 1.1	3	1.00	0.48
AL 1.2	4	0.67	0.32
AL 1.3	5	1.67	0.81
AL 2.1	6	1.00	0.48
AL 2.2	8	1.00	0.48
AL 2.3	9	1.67	0.81

Table 4. Capacitor bank from Feeder 1 and 2.

Capacitor	Bus	Q (Mvar)
AL 1.1	3	1.2
AL 1.2	4	1.2
AL 1.3	5	1.2
AL 2.1	6	0.6
AL 3.2	9	0.6

For this work, the DG was modeled both as SHP as well as PVS, so that different values of inertia could be achieved and the analysis of their impact on islanded systems be more complete. Their respective models are explained in the next sections.

3.1 Synchronous Generator and Governors

The modeling of the synchronous machine and their respective speed governors and voltage regulators are used both by the SHP connected at the end of Feeder 1 and in the case where the DG connected at the end of Feeder 2 is also a SHP. The values and models presented here are based on existing models in Simulight.

Synchronous Generator The dynamic model of the Synchronous Generator used for this study is Model 2 of ANATEM. In it, the user enters the values of the synchronous reactance, in addition to their respective time constants. As it is a single-phase model with a three-phase equivalent, it is necessary to inform the values of resistances and inductances of negative and zero sequence (Zhong and Weiss, 2009). Table 5 displays the values used in this work.

Regarding the inertia constant H of this generator, values 2, 3 and 4 seconds are adopted. Those are typical values of inertia constants for SHP generators. In this way, it is possible to analyze the impacts of different values of inertia on island systems.

Table 5. Model of synchronous machine used for SHPs.

Parameter	Value
H	[2,3,4] s
D	0
S_{base}	6 MVA
r	0.3
x_d	91.1
x_q	58
x_l	0
x_{ld}	40.8
x_{lld}	32.9
T_{ldo}	4.2 s
T_{lldo}	0.04 s
T_{llqo}	0.06 s
R_{neg}	10
X_{neg}	40
R_{zer}	0
X_{zer}	8
R_{ntr}	0
X_{ntr}	0

Speed Governor The speed governor model and parameters are shown in Figure 2 Table 6, respectively.

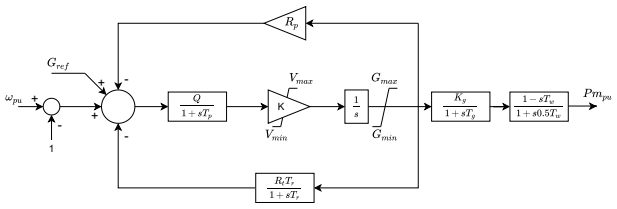

Figure 2. Block diagram of generator's speed governor and hydraulic turbine.

Table 6. Synchronous Generator's speed governor.

Parameter	Value
R_p	0.04 pu
R_t	0.72 pu
Q	1 pu
K	5 pu
T_p	0.05 pu
T_s	1 pu
T_r	9 pu
K_g	1 pu
T_g	0.2 pu
V_{min}	-0.16 pu
V_{max}	0.16 pu
G_{min}	0 pu
G_{max}	1 pu
G_{ref}	0.02204 pu
T_w	2 pu

Voltage Regulator The voltage regulator used here is the IEEE AC5A-A, as pictured in Figure 3. The detailed information is found in IEEE (2006). Typical values for this regulator were adopted, as shown in Table 7.

3.2 Photovoltaic System

The model used to represent the PVS is PVD1, proposed in Force (2014). It is an equivalent phasor model of

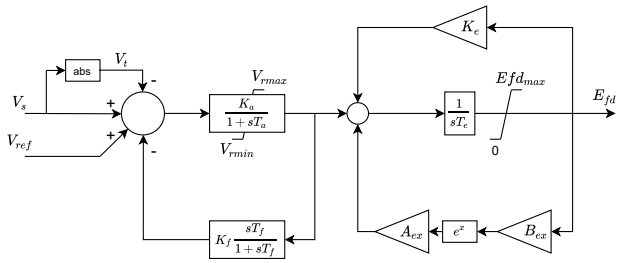

Figure 3. Block diagram of IEEE AC5A-A excitation system.

Table 7. Synchronous Generator's voltage regulator.

Parameter	Value
K_a	400 pu
T_a	0.02 pu
T_e	0.8 pu
K_e	1 pu
K_f	0.03 pu
T_f	1 pu
A_{ex}	0.09826 pu
B_{ex}	0.38737 pu
V_ref	0.98223 pu
E_{fdmax}	200 pu
V_{rmax}	7.3 pu
V_{rmin}	-7.3 pu

a complete photovoltaic module and power electronic converter, thus, the effects of switching and harmonics are not considered. The purpose of this model is to simulate multiple plants or just a small photovoltaic plant, where its control can portray its dynamic behavior (Tang et al., 2013). Figure 4 illustrates the control diagram of this plant, and Table 8 shows the input parameters used in this study.

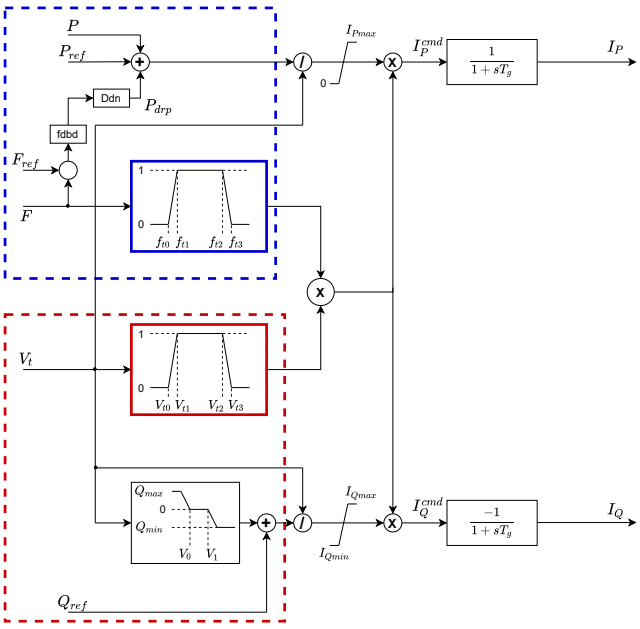

Figure 4. Block diagram of WECC's PVD1 photovoltaic model.

The PVD1 model has blocks that define the operation according to voltage and frequency limits. Outside these

Table 8. Control parameters for WECC's PVD1 model.

Parameter	Value
S_{base}	6 MVA
PQ_{flag}	1
I_{max}	1.1 pu
X_c	0 pu
Q_{max}	0.328 pu
Q_{min}	-0.328 pu
V_0	0.97
V_1	1.03
D_{qdv}	0
f_{dbd}	0.004 pu
D_{dn}	33.3
V_{t0}	0.88 pu
V_{t1}	0.9 pu
V_{t2}	1.1 pu
V_{t3}	1.12 pu
f_{t0}	0.92 pu
f_{t1}	0.95 pu
f_{t2}	1.05 pu
f_{t3}	1.08 pu
T_g	0.02 s

limits, the panel will not produce the currents I_p and I_q, responsible for the injection of active and reactive powers, respectively. Within these limits, the panel will inject I_p and I_q in its entirety if the terminal voltage is between the limits V_{t1} and V_{t2}. A fraction of current between $0 < k < 1$ will be injected if the voltage is between V_{t0} and V_{t1} or between V_{t2} and V_{t3}. The same happens with the frequency limiting block.

In addition to this characteristic, the model also allows the implementation of frequency and voltage droop constants, f_{bdb}, and D_{qdv}, respectively. In this way, the model is capable of sharing active and reactive powers between different generating units.

4. SIMULATION AND RESULTS

Simulation results of the proposed system in Simulight environment are exposed and discuted in this section. For all cases, the same sequence of events were applied, in order to compare the different values of inertia constant. The events occur in the following order:

- t=0 s : system in normal operation;
- t=10 s : interconnection between Feeders 1 and 2 by closing the "DJ-Connection" circuit breaker;
- t=10.5 s : creation of the Feeders 1 and 2 island with the rest of the system by opening the "DJ-SE", "DJ-AL3" and "DJ-BCP" circuit breakers;
- t=130 s : three-phase short circuit solidly grounded in the middle of the "AL-PCH-2" line;
- t=130.1 s : protection of the defective line by opening the "PCH-A" and "PCH-B" circuit breakers;
- t=131 s : extinction of the fault;
- t=250 s : line reconnection;
- t=300 s : end of the simulation.

Figure 5 illustrates the islanded system and the location of the fault (t=130 s)

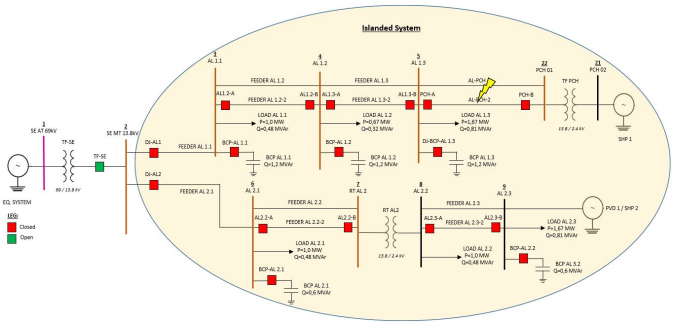

Figure 5. Detail of the topology of the islanded system.

4.1 SHP + SHP System

The results shown here are for the island system operating with two SHPs. The SHP connected to the end of Feeder 1 is called SHP1, while the one connected to the end of Feeder 2 is called SHP2.

Three different cases were simulated, all respecting the events described above, varying the inertia of SHP1 and SHP2 equally in the values of $H = 2s$, $H = 3s$ and $H = 4s$. Thus, the total inertia values of the system are used during the discussion of the results, i.e., $H_{eq} = 4s$, $H_{eq} = 6s$ and $H_{eq} = 8s$. The models of the generators, voltage and speed governors are the same for SHP1 and SHP2.

Figure 6 shows the system frequency during the entire simulation, with different simulated inertia values. Figures 7 and 8 show the post-island and post-defect oscillations in the transmission line, respectively. The blue color represents the results obtained for the system with $H_{eq} = 4s$, red $H_{eq} = 6s$ and green $H_{eq} = 8s$.

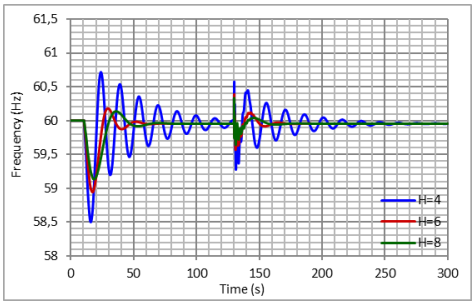

Figure 6. System's frequency for different values of inertia constant.

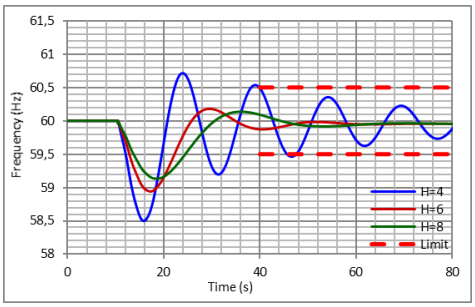

Figure 7. System's frequency for different values of inertia constant after disconnecting from utility grid.

For $H_{eq} = 4s$, the system presented an oscillatory behavior, surpassing the limits of ± 0.5 Hz for more than 30s

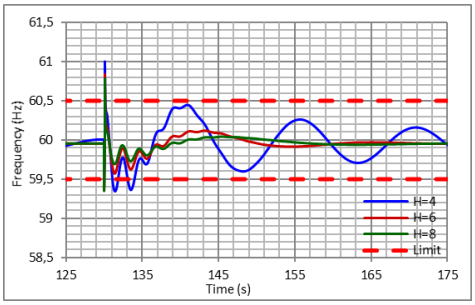

Figure 8. System's frequency for different values of inertia constant after the symmetrical fault.

(ANEEL, 2018), despite reaching steady state stability. As for $H_{eq} = 6s$ and $H_{eq} = 8s$, the system showed small oscillations, but within acceptable limits and reached stability more quickly and satisfactorily when compared to $H_{eq} = 4$s.

The difference between the cases $H_{eq} = 6s$ and $H_{eq} = 8s$ lies in the minimum frequency and the laying time, shown in Figure 7, and in the maximum frequency and the respective settlement time after the defect, shown in Figure 8. In both cases analyzed, $H_{eq} = 8s$ had better results, as expected.

Figures 9 and 10 show the voltages in the connection bus and the SHP1 bus throughout the simulation period, respectively. It is noticed that, in general, for the different H_{eq} there were not many differences in the voltage profile of these key buses.

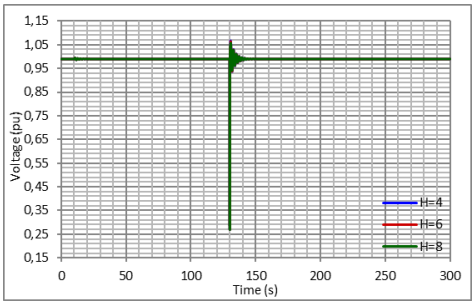

Figure 9. Voltage profile in the connection bus for different values o inertia constant.

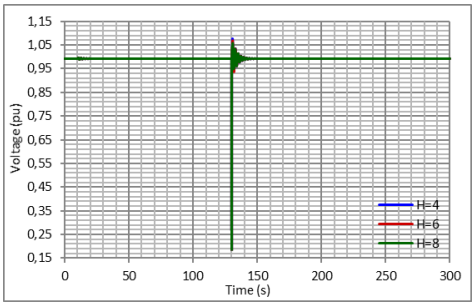

Figure 10. Voltage profile in the SHP1 bus for different values o inertia constant.

Figures 11 and 12 show, in detail, the voltages on the PCH1 bus during islanding and after the fault, respectively.

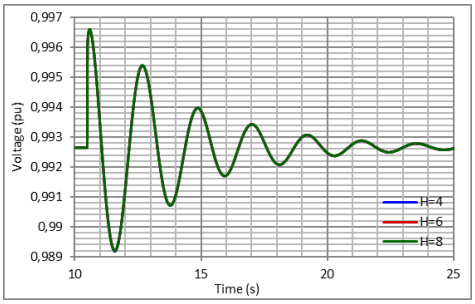

Figure 11. Voltage profile in the SHP1 bus for different values o inertia constant after disconnecting from the utility grid.

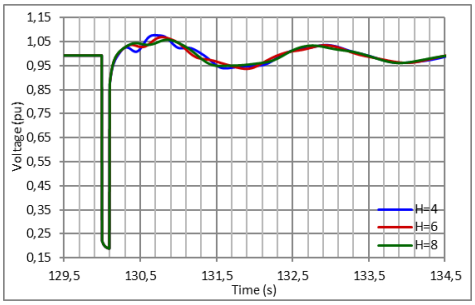

Figure 12. Voltage profile in the SHP1 bus for different values o inertia constant after the symmetrical fault.

Looking closely at the voltage levels in the SHP1 bus, it is clear that after the islanding there is no visual difference between the cases $H_{eq} = 4s$, $H_{eq} = 6s$ and $H_{eq} = 8s$, as shown in Figure 11.

After the defect applied in 130 s, it is possible to notice some differences among the various H_{eq}. Although the settling times are similar, it is possible to notice the presence of small oscillations as the equivalent inertia of the system reduces.

Figures 13 and 14 illustrate the dynamics of the active power injected by SHP1 and the mechanical power on the shaft of the machine, respectively. Again, the presence of faster and less damped oscillations with less inertia is perceived, while with greater inertia stability is achieved quickly. At Figure 14, during the defect, the machine with the lowest inertia constant has a higher instantaneous value of injected active power, which can cause damage to the shaft due to torsional stress.

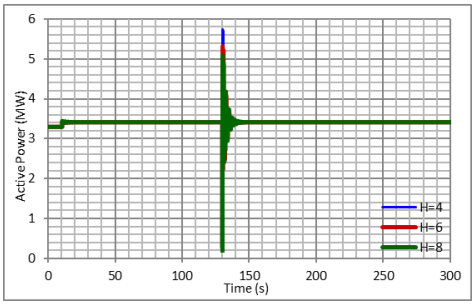

Figure 13. Active power supplied by SHP1.

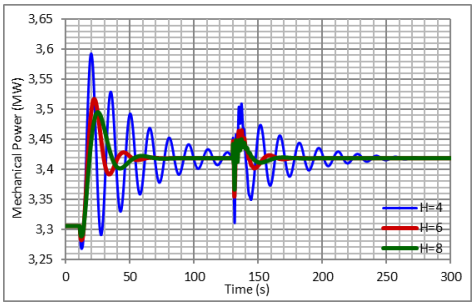

Figure 14. Mechanical power at SHP1's shaft.

4.2 SHP + PVD1 System

The results presented here correspond to the replacement of SHP2 by the PVD1 photovoltaic generation model. As it is a generation without energy storage, the photovoltaic inertia constant is considered to be zero, as it is very small when compared to the inertia of a SHP. In this way, the equivalent inertias H_{eq} are equal to the inertia constants H of SHP1.

$H = 2$ s and $H = 3$ s: For these cases, the respective simulations are only 130 s long, before the three-phase fault is applied. This is because the system is not stable after islanding. Figure 15 shows the frequency of each of the cases collapsing, due to the load-generation imbalance.

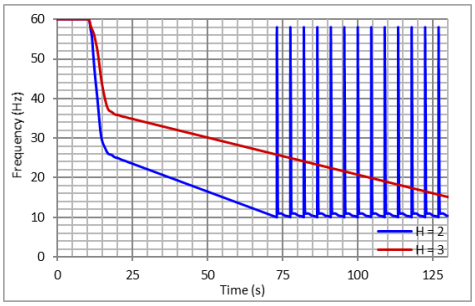

Figure 15. Collapse of the system frequency with PVD1 + SHP1 with $H_{eq} = 2$ and 3.

Figure 16 shows the active power injected by the machine after islanding. Right after this event, the machine goes to the maximum active power that it is able to supply. As this total is less than the island's load, frequency collapse is inevitable.

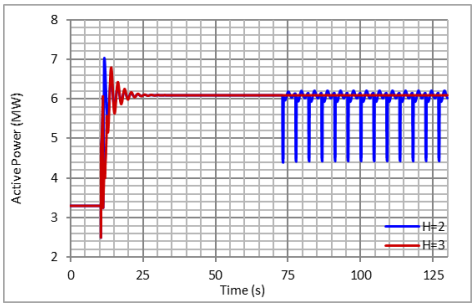

Figure 16. Active power supplied by SHP1.

Figure 17 illustrates the active power injected by PVD1. Before islanding, the panel injects constant power, but

after the event, the frequency value during the first oscillation exceeds the lower limit $ft0$ of the PVD1 control, causing the panel to stop injecting power.

As the values of $H = 2s$ and $H = 3s$ make up a system incapable of recovering from the first oscillation, the frequency of the system continues to decrease, remaining in the power non-injection zone of the panel.

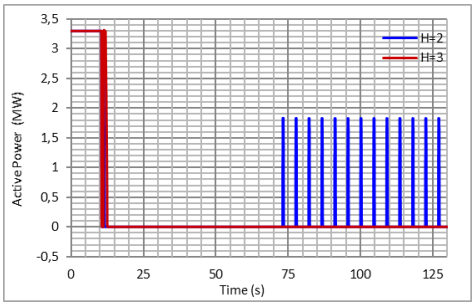

Figure 17. Active power supplied by PVD1.

$H = 4s$: The only case where there was no frequency collapse using the PVD1 model occurred when the SHP1 inertia was $H = 4s$. Unlike the case $H = 2s$ and $H = 3s$, where the frequency collapsed, the system remained intact throughout the simulation period, as shown in Figure 18 .

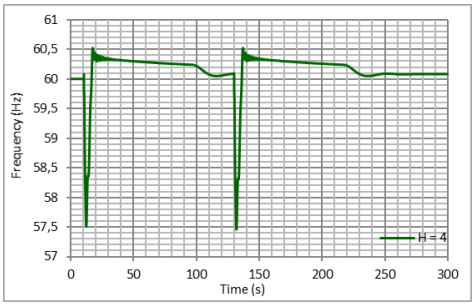

Figure 18. System frequency for the PVD1 + SHP1 scenario with $H_{eq} = 4$.

As the inertia of the SHP is greater, the system remains stable after the first oscillation. Although PVD1 cuts off the injection of active power, the SHP1 generator is able to counter the oscillation. As soon as the PVD1 lower active power limit is reestablished, the photovoltaic system injects active power again, helping the system to recover the load-generation balance. Figure 19 points to this behavior in both the island and the line defect. In addition, it is possible to see the active power droop control acting, where the solar panel starts to share load with the SHP.

The SHP, PVD1 and connection bus voltages are shown in Figure 20. It is observed that despite being stable, the buses of the system have voltage sags that violate the limits. Because the PVD1 control has been modeled so as not to consider the dynamics in the reactive power, it continues to absorb the reactive power of the system in the same magnitude as when before the islanding, as can be seen in Figure 21.

$H_{eq} = 4s$ Case Comparison: For the purpose of analyzing the influence of inertia in islanded systems, the

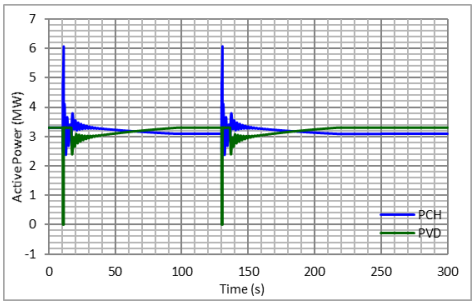

Figure 19. Active power supplied by both the PVD1 and SHP1 generations, for the $H_{eq} = 4$ scenario.

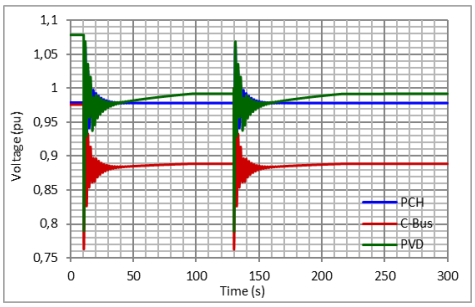

Figure 20. Voltage profile for SHP1, Connection (C-Bus) and PVD1 buses.

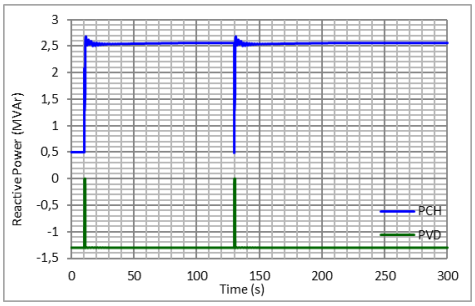

Figure 21. Reactive power supplied by both the PVD1 and SHP1 generations, for the $H_{eq} = 4$ scenario.

system with SHP1 was compared with $H = 4s$ in the $SHP + PVD1$ system and $H = 2s$ for each of the SHP1 and SHP2 in the $SHP{+}SHP$ system. It is, then, the worst case of $SHP + SHP$ with the best case $SHP + PVD1$, both with $H_{eq} = 4s$. Figure 22 shows the frequency of these systems.

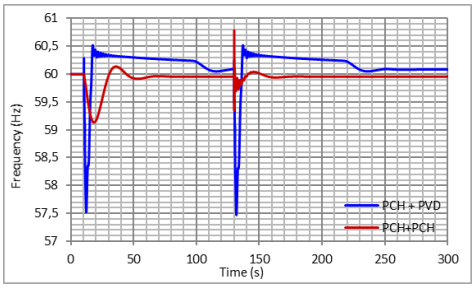

Figure 22. Comparison of system frequencies for both SHP1+SHP2 and PVD1+SHP1 with $H_{eq} = 4$ scenario.

Despite having a more significant drop in frequency during transients, the system with $SHP + PVD1$ returns to

acceptable frequency levels more quickly than the system with the two SHPs. However, the $SHP+SHP$ system has a much shorter settling time than the system with PVD1. In addition, the steady-state frequency of the system with two SHPs is closer to the desirable 60 Hz, compared to the system with PVS.

5. CONCLUSION

With the present work, it was possible to analyze the impact of different values of inertia in islanded systems. Six different values were simulated, also varying the types of generation present in the island.

For the results with two SHPs operating together on the network, it was shown that the impact of inertia on the frequency is direct and explicit, easy to perceive and measure, as expected. As for systemic voltage levels, it is possible to perceive a subtle influence of inertia in the profiles presented, however not as clear as in frequency. Although the system has a $\frac{X_l}{R}$ ratio close to 1, the decoupling of P-f and Q-V can still be considered for the analyzes, in this case.

As for the results of a SHP operating in conjunction with PVS, the influence of inertia values is even more noticeable. In cases with lower values of inertia, the system collapsed due to the load-generation imbalance. With the highest value of inertia in the SHP, the system remained intact, but with unacceptable voltage values. Possible solutions to this problem are implementations of more advanced control techniques and energy storage systems, capable of providing inertia to the system.

It is concluded with this work that inertia is vital for the frequency and voltage profiles of island networks subjected to disturbances. The need for steady generation is also a factor that directly influences the stability of the system.

ACKNOWLEDGEMENTS

We would like to thank Prof. Glauco Taranto from COPPE/UFRJ for the helpful discussions.

REFERENCES

ANEEL, P.d.D.d.E. (2018). Procedimentos de distribuição de energia elétrica no sistema elétrico nacional - PRODIST: Módulo 8 - qualidade de energia elétrica. *Revisão 10*.

Barklund, E., Pogaku, N., Prodanovic, M., Hernandez-Aramburo, C., and Green, T.C. (2008). Energy management in autonomous microgrid using stability-constrained droop control of inverters. *IEEE Transactions on Power Electronics*, 23(5), 2346–2352.

Blaabjerg, F., Teodorescu, R., Liserre, M., and Timbus, A.V. (2006). Overview of control and grid synchronization for distributed power generation systems. *IEEE Transactions on industrial electronics*, 53(5), 1398–1409.

Dag, O. and Mirafzal, B. (2016). On stability of islanded low-inertia microgrids. In *2016 Clemson University Power Systems Conference (PSC)*, 1–7. IEEE.

Delghavi, M.B. and Yazdani, A. (2011). An adaptive feedforward compensation for stability enhancement in droop-controlled inverter-based microgrids. *IEEE Transactions on Power Delivery*, 26(3), 1764–1773.

Force, W.R.E.M.T. (2014). Wecc pv power plant dynamic modeling guide. *Western Electricity Coordinating Council*.

Green, T.C. and Prodanović, M. (2007). Control of inverter-based micro-grids. *Electric power systems research*, 77(9), 1204–1213.

IEEE (2006). IEEE recommended practice for excitation system models for power system stability studies. *IEEE Std 421.5-2005 (Revision of IEEE Std 421.5-1992)*, 1–93. doi:10.1109/IEEESTD.2006.99499.

Katiraei, F. and Iravani, M.R. (2006). Power management strategies for a microgrid with multiple distributed generation units. *IEEE transactions on power systems*, 21(4), 1821–1831.

Kundur, P., Balu, N.J., and Lauby, M.G. (1994). *Power system stability and control*, volume 7. McGraw-hill New York.

Majumder, R., Ghosh, A., Ledwich, G., and Zare, F. (2009). Angle droop versus frequency droop in a voltage source converter based autonomous microgrid. In *2009 IEEE Power & Energy Society General Meeting*, 1–8. IEEE.

Pogaku, N., Prodanovic, M., and Green, T.C. (2007). Modeling, analysis and testing of autonomous operation of an inverter-based microgrid. *IEEE Transactions on power electronics*, 22(2), 613–625.

Sao, C.K. and Lehn, P.W. (2008). Control and power management of converter fed microgrids. *IEEE Transactions on Power Systems*, 23(3), 1088–1098.

Tang, X., Deng, W., and Qi, Z. (2013). Investigation of the dynamic stability of microgrid. *IEEE Transactions on Power Systems*, 29(2), 698–706.

Teodorescu, R., Blaabjerg, F., Liserre, M., and Loh, P.C. (2006). Proportional-resonant controllers and filters for grid-connected voltage-source converters. *IEE Proceedings-Electric Power Applications*, 153(5), 750–762.

Tielens, P. and Van Hertem, D. (2012). Grid inertia and frequency control in power systems with high penetration of renewables. In *Young Researchers Symposium in Electrical Power Engineering, Date: 2012/04/16-2012/04/17, Location: Delft, The Netherlands*.

Vasquez, J.C., Guerrero, J.M., Miret, J., Castilla, M., and De Vicuna, L.G. (2010). Hierarchical control of intelligent microgrids. *IEEE Industrial Electronics Magazine*, 4(4), 23–29.

Zhang, X., Wang, Y., Fu, Y., and Xu, L. (2016). A novel method for obtaining virtual inertial response of dfig-based wind turbines. *Wind Energy*, 19(2), 313–328.

Zhong, Q.C. and Weiss, G. (2009). Static synchronous generators for distributed generation and renewable energy. In *2009 IEEE/PES Power Systems Conference and Exposition*, 1–6. IEEE.